Journal of Magnetic Resonance **154,** 311–316 (2002)
doi:10.1006/jmre.2001.2495, available online at http://www.idealibrary.com on IDEAL®

COMMUNICATIONS

NMR Velocimetry of Falling Liquid Films

C. Heine, K. Kupferschläger, S. Stapf, and B. Blümich

Institute of Technical Chemistry and Macromolecular Chemistry, Rheinisch-Westfälische Technische Hochschule, D-52056 Aachen, Germany

E-mail: sstapf@mc.rwth-aachen.de

Received May 21, 2001; revised November 16, 2001

First results on NMR velocimetry of falling liquid films are presented. A film of average thickness 1 mm and width 40 mm is sustained by a continuous flow of silicon oil over a vertical plate made from PMMA. The spatial distribution of velocities is measured using a double spin–echo imaging pulse sequence supplemented by a bipolar velocity encoding gradient. Spin density and velocity images as well as two-dimensional velocity maps of different situations, i.e., undisturbed and disturbed falling film flow, are discussed. Experimental and theoretical velocity data for undisturbed film flow are compared. © 2002 Elsevier Science (USA)

1. INTRODUCTION

A film flow is defined as a liquid layer falling down at least one free boundary under the effect of gravity and shear stress (*1*). The thickness of such films is on the order of 0.1 to 1 mm. Falling films are important for industrial applications, e.g., condensers and evaporators, and in the context of extraction. Typical implementations of falling film flow are annular flow along the internal surface of a tube and flow along an inclined plane (*1*). One characteristic feature of falling films is the natural appearance of nonlinear surface waves at very low Reynolds numbers $\mathrm{Re_f}$. $\mathrm{Re_f}$ characterizes the flow behavior. It is inversely proportional to the viscosity η of the fluid,

$$\mathrm{Re_f} = \frac{\rho v_z h}{\eta}, \qquad [1]$$

where ρ is the density of the fluid, v_z the velocity component in the direction of gravity, and h the film thickness. A critical Reynolds number, $\mathrm{Re_c}$, can be predicted from theory (*2*). Waves should occur for $\mathrm{Re_f} \geq \mathrm{Re_c}$, while the film should be laminar and waveless for $\mathrm{Re_f} < \mathrm{Re_c}$. For laminar films waves can be excited by a periodic disturbance. There are several realizations of such disturbances, e.g., acoustic stimuli (*2, 3*), pulsatile flow (*1*), or the oscillating wire technique (*4*). These waves change the properties of mass and heat transfer in two-phase film flow. Thus for the optimization of industrial applications of film flow a basic understanding of the hydrodynamics of single and multiphase film flow is essential.

Nusselt predicted a parabolic dependence of the velocity component v_z in the direction of gravity versus the coordinate through the film x (*5*),

$$v_z(x) = \frac{\rho g h^2}{2\eta}\left(2\frac{x}{h} - \frac{x^2}{h^2}\right), \qquad [2]$$

where g is the earth's acceleration constant. This equation was deduced for laminar flows with $\mathrm{Re_f} \ll 1$, but it was proven to be valid for all laminar film flows (*1*). Equation [2] corresponds to a maximum velocity at the surface of the film of

$$v_{z,\max} = \frac{1}{2}\frac{\rho g h^2}{\eta} \qquad [3]$$

and to an average velocity across the film of

$$\bar{v}_z = \frac{\rho g h^2}{3\eta}. \qquad [4]$$

Until now mainly optical methods have been implemented to measure velocities and film thickness. Most of them are based on the use of tracers (e.g., (*6–8*)), laser doppler anemometry (e.g., (*9–11*)), or particle image velocimetry (*3*). None of these techniques is chemically selective. Therefore NMR measurements are highly desirable, in combination with spatial resolution (*12, 13*) and the ability to perform velocity measurements (*14*).

In this work we report our first results of NMR velocimetry of thin falling liquid films, less than 1.5 mm thick. To our knowledge, until now there have been no published results measured by means of NMR for a system like this.

2. EXPERIMENTAL

The device used for generation of falling liquid films is sketched in Fig. 1. It is constructed of polymethylmethacrylate

1090-7807/02 $35.00

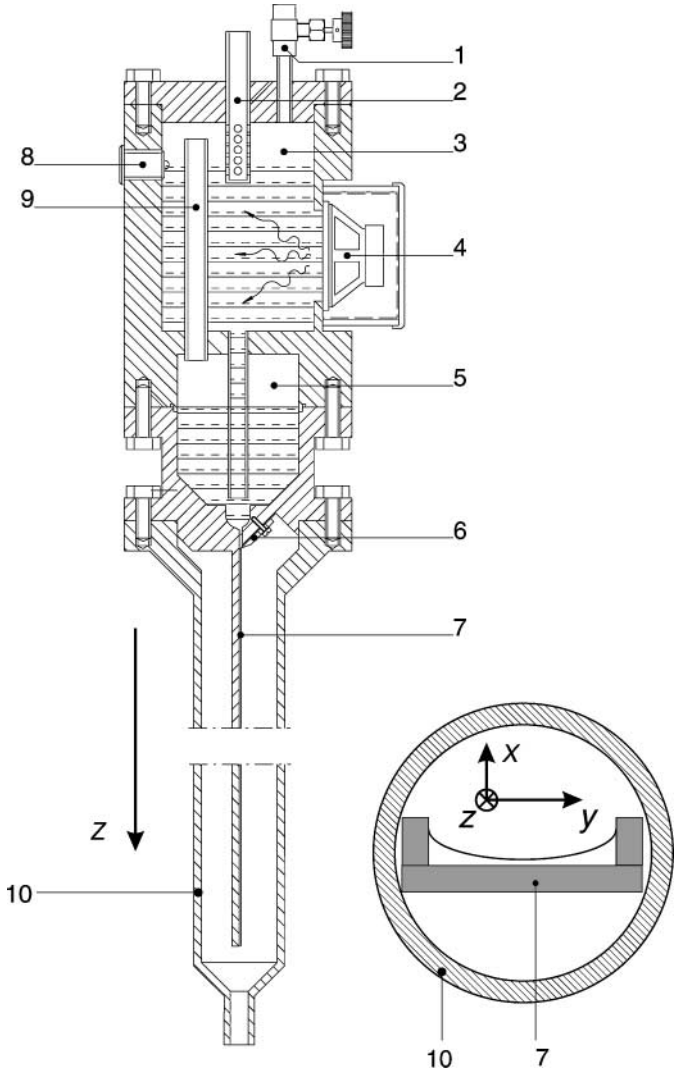

FIG. 1. Drawing of the falling film device. The film is falling along a 40-mm-wide plate (7) made from PMMA. The film is generated using a straight adjustable blade (6) that allows control of the film thickness. The device contains two reservoirs (3, 5), inlets (2, 9), and pressure-equalizing gauges (1, 9). It allows the application of acoustic waves on the reservoir using the loudspeaker (4) to excitate waves on the film. A level-controlling device (8) is implemented that regulates the supply pump in case the filling level of the reservoir exceeds a maximum value. The flow direction is the *z* direction. The inset shows a transverse section through the lower part of the device with the tube (10) and the plate (7), as well as the definition of the axes used in this work: *x* through the film, *y* along the film, and *z* along the falling direction. The plate is shaped in the form of a U.

(PMMA) and consists of a tube of outer diameter 64 mm which is stabilizing a 40-mm-wide vertical plate of length 75 cm. The fluid is flowing on one of the surfaces of this plate. The tilt of the plate can be adjusted within $\pm 3^\circ$ and was set to be perfectly vertical for the experiments described in this work. The maximum deviation from vertical orientation is estimated to be 0.5°. The sensitive volume is located 50 to 60 cm below the beginning of the plate, allowing maximum time for the equilibration of the film flow. The average film thickness is adjustable by varying the separation of a blade from the PMMA plate. The direction of the flow, i.e., the direction of the gravitational forces driving the flow, defines the *z* direction, the direction "through" the film is the *x* direction, and the one "along" the film is the *y* direction (cf. Fig. 1). The falling film device is constructed in such a way as to maintain the possibility of driving the film as an open or closed system, i.e., either allowing pressure compensation or not.

There are two different fluid reservoirs separated from each other in order to avoid pulsatile flow components from direct connection to a pulsatile pump. Furthermore, this separation of reservoirs results in a constant pressure in the second reservoir and therefore at the position of the film initiation.

The device includes a loudspeaker that can be used to excite two- or three-dimensional waves in the film depending on $\mathrm{Re_f}$, i.e., waves that extend over two dimensions and are constant over the third or waves that extend over three dimensions, respectively. The properties of these wavy films depend on the flow velocity, the film thickness, and the material properties of the flowing liquid (*1*). However, wavy films are also generated using excess pressure. This requires a closed system, i.e., a system where no pressure compensation of the system with the environment is possible. In this case the pump is applied in such a way that excess pressure is generated in the reservoirs and low pressure is generated in the tube containing the PMMA plate by removal of liquid from the bottom end. If a pulsatile pump is used, this generates waves on the film.

All experiments were performed at room temperature. As a sample fluid PDMS (polydimethylsiloxane) has been chosen, because the NMR spectrum consists just of a single line and it provides a favorable opportunity for studying the influence of viscosity on the flow without the necessity of adding fluids which contribute a different spectral signature. The experiments were performed with silicon oil BaySilone M100 produced by *Bayer* with a viscosity of $\eta = 97$ mPa s and a density of $\rho(25^\circ\mathrm{C}) = 0.97\ \mathrm{g/cm^3}$. The viscosity of the oil is nearly 100 times higher than that of water, so the flow is rather slow and outflow effects are reduced.

The NMR measurements were performed in a 4.7-T 150-mm-bore vertical superconductive magnet, driven by a *Bruker DSX-200* console, using a Mini 0.36 gradient system with a 64-mm inner diameter birdcage resonator. A maximum resolution of 90 μm per pixel in readout direction, which was chosen across the thickness *x* of the film, was achieved. For velocity mapping we have employed the phase encoding pulse sequence shown in Fig. 2 (*14, 15*). The use of two π pulses is recommended, because phase shifts due to background gradients are refocused. In this figure the velocity filter, a bipolar gradient pair in between the two π pulses, is shown in the read direction, whereas it can be implemented in any direction. The result of this bipolar gradient pair is a phase shift of the moving spins in addition to the usual phase shift in *k* space imaging proportional

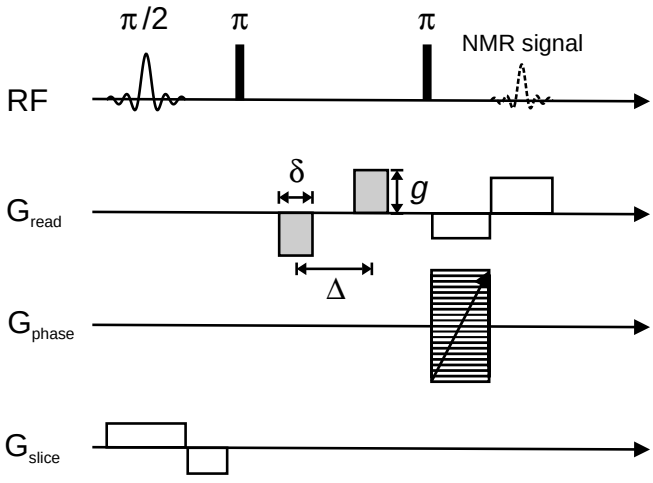

FIG. 2. Pulse sequence for phase encoding of velocities. The bipolar velocity-encoding gradient pair is shown shadowed in the read direction. It can be implemented in any desired spatial direction. g is the strength of the gradient pair, δ is the length of one of the pulses, and Δ is the pulse separation (*14, 15*).

to q (*12*), where

$$q = \frac{\gamma}{2\pi} g \cdot \delta, \qquad [5]$$

g is the amplitude of the bipolar gradient pair, and δ is the pulse length of one of the two gradient pulses, as indicated in Fig. 2. This phase shift is given by

$$\Delta\phi = 2\pi q R, \qquad [6]$$

where R is the spin displacement during the gradient pulse spacing time Δ. In principle it is sufficient to compare images obtained for two different values of q and to eliminate static phase shifts which are independent of the application of the bipolar gradient pair. Such static contributions can arise, e.g., from susceptibility differences in the sample or from eddy currents. However, to improve the reliability of the measurements, nine different q values were chosen in the range from $-q_{\max}$ to $q_{\max}$. The results presented here were acquired with $\delta = 2$ ms and $\Delta = 4$ ms (cf. Fig. 2).

Furthermore we employed a single stripe tagging technique (*16, 17*). A thin slice in the z direction is excited with a slice-selective $\pi/2$ pulse. Following a time delay τ a conventional spin-warp imaging pulse sequence is started. The magnetization of the slice is stored in the z direction by the initial $\pi/2$ pulse of the spin-warp sequence. Thus the resulting image includes a tagged slice essentially without magnetization depending on τ. By varying τ the flow behavior can be visualized. The results presented here consist of a tagged slice of width 2 mm and τ in the range from 0 to 200 ms.

3. RESULTS

A spin density image of the y–z plane of waveless falling film flow is depicted in Fig. 3. A variation of the thickness in the y direction is detected, which is due to surface tension effects that increase the thickness of the film toward the side boundaries of the plate. Figure 3 reveals a region of about 10-mm width where the film is nearly flat and waveless. There the film exhibits a thickness of 1.0 mm. This means that by imaging slices in the y direction with widths not exceeding 10 mm one images the flat region without the need to consider boundary effects. The curved shapes at the boundaries of the image are a consequence of distortions resulting from the particular resonator used. The bright "spot" in the center of the image results from a DC artefact at the crossing point of the lines indicating zero frequency after Fourier transformation; the high intensity at this point has been set to zero.

Figure 4 shows a velocity map of undisturbed film flow at $\mathrm{Re_f} = 1.2$. In order to obtain this map two velocity components, v_z and v_y, were measured spatially resolved in the y and z directions and combined to produce this vector plot. The velocity map reveals the fact that the flow is much faster in the regions of greater film thickness near $y = 10$ and 40 mm. This can be understood by considering the fact that even in the laminar flow case both the surface and the average velocity are faster if the film thickness h is greater. Following Eqs. [3] and [4] higher flow velocities in the edge regions result for increasing h, and both the surface velocity and the velocity averaged with respect to x increase. At $\mathrm{Re_f} = 1.2$ waves should already appear, because for the silicon oil used $\mathrm{Re_c} = 0.9$ is valid. As the data in Fig. 4 are not spatially resolved in the x waves would just change the averaged velocity $\bar{v}_z$. In the center region, the velocity component v_z averaged with respect to x amounts to $\bar{v}_{z,\mathrm{center}} = 75$ mm/s, which is in good agreement with the results of single slice tagging

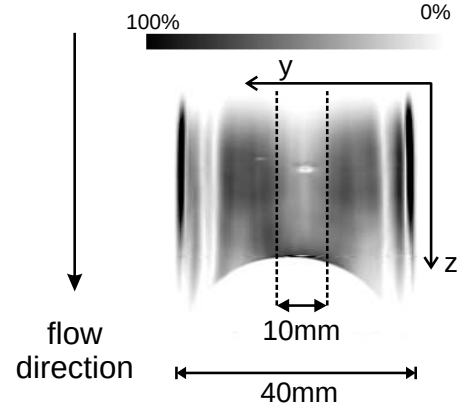

FIG. 3. y–z spin-density image of a waveless falling film. The film thickness is approximately 1.0 mm. No wave is visible. A variation in the film thickness can be observed, due to the surface tension and the U-shape of the falling film plate (cf. Fig. 1). The film thickness increases at the edges of the plate. The region of film flow without boundary effects is about 10 mm wide.

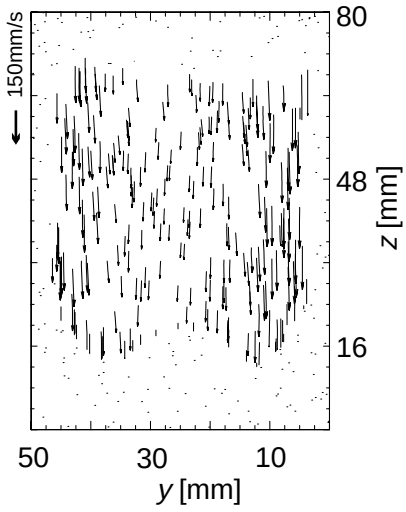

FIG. 4. Two-dimensional y–z velocity map of an undisturbed falling liquid film at $\mathrm{Re_f} = 1.2$. Magnitude and direction are represented as velocity vectors. The flow is faster at the edges of the plate, due to creep of the silicon oil. The velocity vectors are nearly parallel to the z direction at all locations.

experiments. Most particles move parallel to each other. This results in an average velocity of zero in the y direction, which is indeed observed within the precision and accuracy of the experimental data.

Figure 5 shows the results of single slice tagging experiments at $\mathrm{Re_F} = 1.2$. A sequence of images is shown, with increasing τ, the time between the tagging and the start of the imaging sequence. The delay τ is varied between 0 and 200 ms. The faster flow, corresponding to the larger film thickness at the edges of the plate, is visible as well as the slower flow in the center and a region of slow flow in between the two. The flow in the edge regions is so fast that even during tagging (which takes approximately 1 ms) the particles move from pixel to pixel, as can be seen in the distorted pattern near the edges for $\tau = 0$.

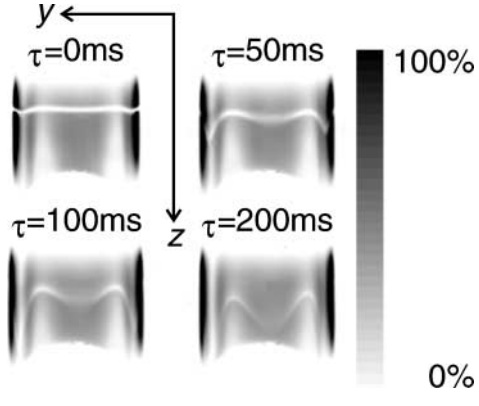

FIG. 5. Tagging experiments on undisturbed film flow at $\mathrm{Re_f} = 1.2$. τ symbolizes the time between the tagging of a single slice of width 2 mm along z and the beginning of the imaging experiment. It can be seen clearly that the flow near the edges of the PMMA plate is faster than that at the center.

At $\tau = 200$ ms the fastest components have already left the sensitive volume of the birdcage. These tagging images confirm that for the measurement of velocities spatially resolved in x direction a thin slice centered with respect to y in the middle of the film should be used. Surface waves have no direct impact on the tagging images, because these have no spatial resolution in x.

Figure 6 shows v_z versus x for two different $\mathrm{Re_f}$. Figure 6a was measured at $\mathrm{Re_f} = 0.5$, which is well below the critical Reynolds number, $\mathrm{Re_c} = 0.9$. This means the film is in the laminar flow regime. The experimental data (shown as diamonds) follow a parabola. The data can be approximated by Eq. [2] with reasonable parameters. The fit is plotted as a solid line. The film thickness is 1.0 mm, identical to the one at film initiation. With increasing $\mathrm{Re_f}$, the situation changes. For $\mathrm{Re_f} = 1.3$ as shown in Fig. 6b the experimental data cannot be fitted to a simple parabola but to two parabolas in distinct areas. The apparent film thickness increases to approximately 1.3 mm. This can be explained by the natural appearance of waves, because $\mathrm{Re_f} > \mathrm{Re_c}$ applies. The film behavior is laminar-wavy but not turbulent, which would be expected for $\mathrm{Re_f} > 75$ (*18*).

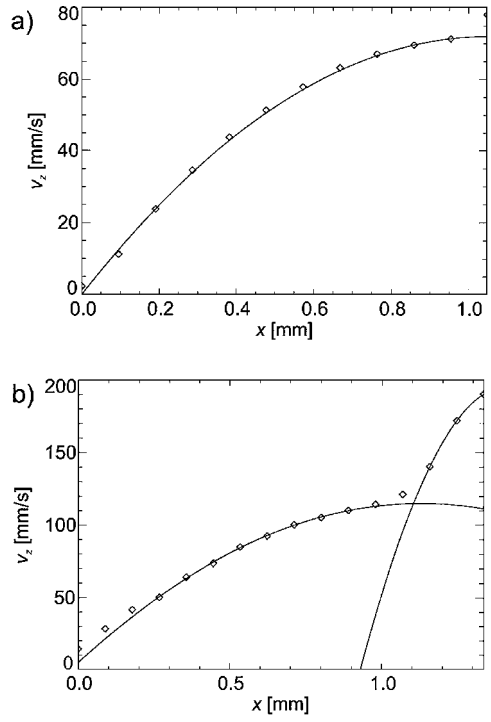

FIG. 6. Flow velocity components v_z versus position x across the film thickness for different $\mathrm{Re_f}$. (a) $\mathrm{Re_f} = 0.5 < \mathrm{Re_c}$. In this case the film is laminar and the velocity is described by Eq. [2]. The film thickness is 1 mm, which is equivalent to the thickness at the film initiation. (b) $\mathrm{Re_f} = 1.3 > \mathrm{Re_c}$. The film is laminar-wavy. The experimental data (shown as diamonds) can be described by two parabolas. One parabola, extending from $0 \leq x \leq 0.9$ mm, is due to the residual film; the other, for 1.1 mm $\leq x \leq$ 1.3 mm, is due to the averaged waves.

Such a wavy film is divided into two parts with respect to x. Underneath the waves exists a residual film that behaves quasi-laminar, thus showing a parabolic velocity profile following Eq. [2]. It is measured in the region of $0 \leq x \leq 0.9$ mm. Each single wave also exhibits a parabolic velocity profile itself (*3*). When analyzing the data one has to keep in mind that the waves are measured in a time-averaged fashion, as it is not easily possible to trigger to the waves because of their spontaneous appearance. Thus in every single scan a wave is measured in a different state. This means that the parabola in the second region ($1.1\,\text{mm} \leq x \leq 1.3$ mm) is due to time-averaged waves. The intermediate region ($0.9\,\text{mm} < x < 1.1$ mm) is due to small fluctuations in the residual film thickness. Both Figs. 6a and b show a small deviation of the fit functions near the plate, which is situated at $x = 0.0$ mm. This is due to the sudden change of magnetic susceptibility at this point. All in all the NMR data prove the validity of the critical Reynolds number Re_c.

In the case described above the system was driven in an open manner; i.e., pressure balancing of the film flow device with the environment was possible. In order to investigate the feasibility of measuring flow behavior in films in the presence of standing waves, the system was driven as a closed circuit as described above. Figure 7 shows a spin-density image of such wavy film flow. The triangular wave in the center of the image is clearly visible and could also be seen during the experiment by optical inspection. The two strong signals at the edges of the film plate are due to creep of the silicon oil. The wave was generated by sealing the system against the environment, applying excess pressure (i.e., low pressure in the tube) and by using a pulsatile pump. If the system is opened for pressure equalization the film flow is waveless, as discussed above. The wave was stationary over the experimental time, which was about 40 min.

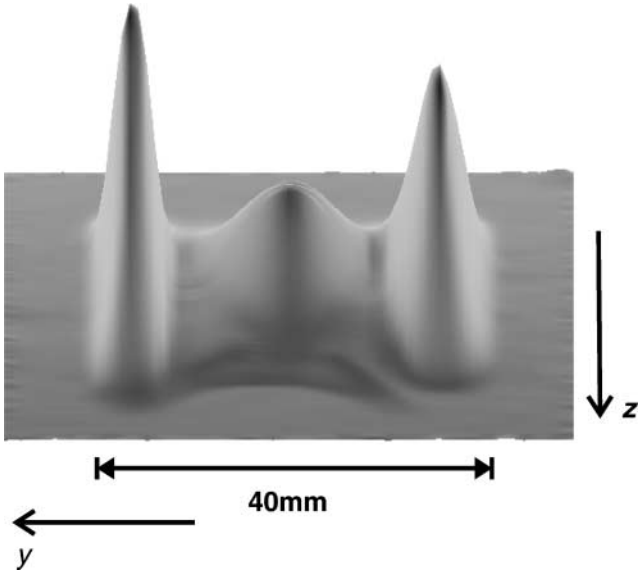

FIG. 7. *y–z* spin-density image of a pressure-induced wavy falling liquid film. The triangular shape of the wave in the center can be clearly seen. The regions with the high signals at the left and right are due to surface tension effects at the edges of the plate confining the film.

4. CONCLUSION

We have demonstrated the general possibility of performing NMR measurements on thin falling liquid films. Velocity maps and images are presented for undisturbed film flow with an averaged thickness of 1.0 mm as well as spin density images of wavy and waveless films. Future work will include one-shot velocimetry measurements (*19*). The results presented here are the first step toward a systematic study of falling film flow by NMR. Introduction of wave excitation by acoustic vibrations, hereby varying both frequency and amplitude, and the use of fluids with different surface tensions will follow.

ACKNOWLEDGMENTS

We are grateful to Peter Blümler for developing the concept of this project. Funding by the Deutsche Forschungsgemeinschaft (SFB 540, "Modellgestützte experimentelle Analyse kinetischer Phänomene in mehrphasigen fluiden Reaktionssystemen") is gratefully acknowledged. The work benefitted from helpful discussions with Song-I Han and Ute Görke.

REFERENCES

1. S. V. Alekseenko, V. E. Nakoryakov, and B. G. Pokusaev, "Wave Flow of Liquid Films," Begell House, New York (1994).
2. P. L. Kapitza, Wave flow of a thin layer of viscous fluid, *Zh. Eksp. Teor. Fiz.* **18,** 3 (1948).
3. P. Adomeit and U. Renz, Hydrodynamics of three-dimensional waves in laminar falling films, *Int. J. Multiphase Flow* **26,** 1183–1208 (2000).
4. T. Nosoko, P. N. Yoshimura, T. Nagata, and K. Oyakawa, Characteristics of two-dimensional waves on a falling liquid film, *Chem. Eng. Sci.* **51,** 725–732 (1996) .
5. W. Nusselt, Die Oberflächenkondensation des Wasserdampfes, *VDI Z.* **60,** 541 (1916).
6. F. C. K. Ho and R. L. Hummel, Average velocity distribution within falling liquid films, *Chem. Eng. Sci.* **25,** 1225–1237 (1970).
7. V. Y. Nakoryakov, B. G. Pokusaev, S. V. Alekseenko, and V. V. Orlov, Instantaneous velocity profile in a wavy fluid film, *J. Eng. Sci.* **33,** 1012–1016 (1977).
8. S. V. Alekseenko, V. Y. Nakoryakov, and B. B. Pokusaev, Wave formation on vertical falling liquid film, *AIChE J.* **31,** 1446–1460 (1985).
9. M. G. Semena and G. A. Mel'nichuk, Mean-velocity distributions in a falling film, *Fluid Mech.-Sov. Res.* **7,** 145–151 (1978).
10. I. Mudawar and R. A. Houpt, Mass and momentum transport in smooth falling liquid films laminarized at relatively high Reynolds numbers, *Int. J. Mass Heat Transfer* **36,** 3437 (1993).
11. I. Mudawar and R. A. Houpt, Measurements of mass and momentum transport in wavy-laminar falling liquid films, *Int. J. Heat Mass Transfer* **36,** 4151 (1993).
12. P. T. Callaghan, "Principles of Nuclear Magnetic Resonance Microscopy," Clarendon, Oxford (1993).

13. B. Blümich, "NMR Imaging of Materials," Clarendon, Oxford (2000).

14. E. Fukushima, Nuclear magnetic resonance as a tool to study flow, *Annu. Rev. Fluid Mech.* **31,** 95–123 (1999).

15. A. Caprihan and J. D. Seymour, Correlation time and diffusion coefficient imaging: Application to a granular flow system, *J. Magn. Reson.* **144,** 96–107 (2000).

16. E. Zerhouni, D. Parrish, W. J. Rodgers, A. Yang, and E. P. Shapiro, Human heart: Tagging with MR imaging—A method for noninvasive assessment of myocardial motion, *Radiology* **169,** 59 (1988).

17. L. Axel and L. Dougherty, Heart wall motion: Improved method of spatial modulation of magnetization for MR imaging, *Radiology* **172,** 349 (1989).

18. S. Ishigai, S. Nakanisi, T. Koizumi, and Z. Oyabi, Hydrodynamics and heat transfer of vertical falling liquid films, *Bull. JSME* **15,** 594 (1972).

19. T. W. J. Scheenen, D. van Dusschoten, P. A. de Jager, and H. van As, Microscopic displacement imaging with pulsed field gradient turbo spin–echo NMR, *J. Magn. Reson.* **142,** 207–215 (2000).